

JGR Space Physics

RESEARCH ARTICLE

10.1029/2020JA027902

Key Points:

- During substorms mid-latitude magnetic variations are highly correlated with the peak auroral electrojet intensity throughout the night side
- Longitudinal structures of midlatitude magnetic variations are organized by the peak location of the westward auroral electrojet intensity
- As a first approximation, the substorm current wedge is a globally coherent system rather than an ensemble of wedgelets

Supporting Information:

- Supporting Information S1

Correspondence to:

S. Ohtani,
ohtani@jhuapl.edu

Citation:

Ohtani, S., & Gjerloev, J. W. (2020). Is the substorm current wedge an ensemble of wedgelets?: Revisit to midlatitude positive bays. *Journal of Geophysical Research: Space Physics*, 125, e2020JA027902. <https://doi.org/10.1029/2020JA027902>

Received 11 FEB 2020

Accepted 22 JUL 2020

Accepted article online 11 AUG 2020

Is the Substorm Current Wedge an Ensemble of Wedgelets?: Revisit to Midlatitude Positive Bays

Shinichi Ohtani¹  and Jesper W. Gjerloev^{1,2} 

¹The Johns Hopkins University Applied Physics Laboratory, Laurel, MD, USA, ²Faculty for Physics and Technology, University of Bergen, Bergen, Norway

Abstract The goal of the present study is to observationally test the idea that the substorm current wedge (SCW) is an ensemble of wedgelets, mesoscale current systems that correspond to plasma sheet flow channels. According to this hypothesis, the *SML* index, SuperMAG equivalent to the *AL* index, represents a single particular wedgelet at a given time, whereas midlatitude positive bays are a sum of the remote effects of all wedgelets but with more weighting on ones closer in longitude. However, both event-based and statistical studies of isolated substorms show that (1) midlatitude *N* (northward) and *E* (eastward) ground magnetic variations are highly correlated with *SML* even far from midnight; (2) the correlation between midlatitude magnetic variations and *SML* are organized by the magnetic local time (MLT) of the peak westward electrojet intensity (as identified by *SML*), and their longitudinal structures are consistent with the conventional SCW model; and (3) eastward and westward midlatitude *E* variations observed at dusk and dawn, respectively, are well correlated. If the SCW is an ensemble of wedgelets, these results would imply that wedgelets with similar intensities are formed side by side throughout the SCW and evolve in parallel with each other, which is highly questionable from both physical and morphological points of view. Instead, it is suggested that the SCW is basically a globally coherent system. Although the SCW may evolve from a wedgelet formed at the onset of substorms, wedgelets are probably not a primary constituent of the SCW for most of the subsequent expansion phase.

1. Introduction

The structure of the substorm current system, the substorm current wedge (SCW), is one of the most fundamental issues of substorm physics. In this study we will observationally test whether the SCW is one coherent system or an ensemble of smaller elements, so-called wedgelets. If the former is the case, the substorm is considered to be the temporal and spatial development of a single large-scale process. In contrast, if the latter is the case, the substorm is considered to be the temporal and spatial superposition of wedgelet formations. Thus, our perspective of substorm dynamics in general would be rather different depending on the result of this test.

The SCW is a model current system, in which a part of the cross-tail current short-circuits through the ionosphere with a pair of field-aligned currents (FACs) (McPherron et al., 1973). The FACs flow into and out of the ionosphere on the downside and duskside, respectively. That is, they have the Region-1 (R1) sense polarity. The ionospheric closure current of those FACs represents the enhancement of the westward electrojet (WEJ). It is possible that the auroral expansion in the ionosphere following substorm onsets reflects the spatial development of the wedge current system (Akasofu, 1972). This idea is appealing especially because the auroral substorm is characterized by the formation and expansion of the auroral bulge (Akasofu, 1964). At the duskside front of the auroral bulge, that is, the westward traveling surge, auroral emission is consistently intense and is collocated with an intense upward FAC (Fujii et al., 1994), which presumably corresponds to the upward FAC of the SCW. The corresponding downward FAC is difficult to identify since it is not associated with any specific auroral structure, and it may be distributed more diffusely. Nevertheless, the WEJ enhancement extends over the entire sector of the auroral bulge (Gjerloev & Hoffman, 2014), which is consistent with the idea that the SCW expands along with the region of auroral intensification.

However, the spatial expansion of auroral substorms is not necessarily continuous, but it can be discrete. Rostoker (1991) suggested that the westward traveling surge, despite its term, actually stays where it

forms, but a new surge appears to the west of the preexisting one at substorm intensifications. Such intensifications may also be accompanied by the poleward and westward leap of the WEJ (Kisabeth & Rostoker, 1974). Here each substorm intensification may be envisioned as an addition of a small-scale wedge current system, that is, wedgelet, to the west of the preexisting current system. Thus, the idea of wedgelets was initially introduced to explain discrete, as opposed to continuous, westward expansion of auroral substorms.

The concept of wedgelets has been generalized, or altered, since then as the formation of plasma sheet flow channels drew growing attention as a recurrent fundamental process of the magnetosphere-ionosphere (M-I) system. Fast earthward flows in the plasma sheet are mapped to the ionosphere as equatorward flows with a pair of R1 sense FACs separated typically 1 hr in magnetic local time (MLT) (Juusola et al., 2009). Auroral streamers are widely considered to be an auroral manifestation of the upward FAC of such a FAC pair (Nakamura et al., 2001; Sergeev et al., 1999), and they are observed inside the auroral bulge during the course of the substorm expansion phase (e.g., Henderson, 2013). Considering all these aspects, it is tempting to consider that the current system associated with plasma sheet flow channels, wedgelet, is a fundamental element of the SCW. This idea also appears to be consistent with the recent result of a global simulation that near-Earth dipolarizations are an accumulation of small-scale magnetic enhancements carried by fast plasma flows from farther down the tail (Merkin et al., 2019).

On the other hand, if the SCW is an ensemble of wedgelets, the WEJ would be segmental unless they form simultaneously side by side. More precisely, each wedgelet should appear as a 2-D dipole-like configuration of equivalent currents (Fukushima, 1971), and therefore, the WEJ would be represented by a series of such 2-D dipole-like equivalent currents as opposed to one coherent structure as historically known as the DP1 current (e.g., Akasofu et al., 1965; Obayashi & Nishida, 1968). The issue may be resolved if individual flow channels have finite net FACs, which tend to flow toward and out of the ionosphere on the dawnside and duskside, respectively, as Liu et al. (2015) suggested based on their satellite data analysis. Whereas those authors emphasized the importance of wedgelets as fundamental elements of the SCW, this idea itself implies that the wedgelets are superposed on the top of a global current system. Here a critical question is to what extent each of the global and mesoscale components contributes to the substorm current system.

In the present study we observationally address the constitution of the SCW by comparing the *SML* index, the SuperMAG equivalent to the *AL* index (section 2), with midlatitude positive bays, ground magnetic disturbances equatorward of the auroral zone. *SML* is a measure of the maximum local WEJ intensity. If the SCW is an ensemble of wedgelets as shown in Figure 1a, *SML* represents one particular wedgelet (WL3 in Figure 1a), whereas midlatitude positive bays are a sum of the remote effects of all wedgelets (WL1–5) but with more weighting on closer ones. It is therefore expected that the correlation of midlatitude bays with *SML* is highest in the MLT sector of *SML*-contributing stations, and it decreases with increasing separation in MLT. This longitudinal dependence should be more sensitive closer to the auroral zone. On the other hand, if the SCW is globally coherent as a first approximation as shown in Figure 1b, the correlation distance would be global; it would exceed the longitudinal extent of the SCW itself since its magnetic effect extends to outside of the SCW.

The objective of this study is to determine which of the two cases shown in Figure 1 better represents the SCW system. We realize that the instantaneous current system is more complex than these configurations. There are many mesoscale and small-scale current systems other than wedgelets, which develop at different spatial and temporal scales. Moreover, the SCW itself develops not only in time but also in space, and accordingly, the *SML*-contributing station moves. This dynamic nature of substorms should generally reduce the correlation between *SML* and midlatitude positive bays, but the reduction would be likely more pronounced if the SCW is an ensemble of wedgelets. We also note that whether *SML* represents a local wedgelet or the entire SCW, our approach assumes that *SML* is a measure of the total current of the corresponding current system. (If *SML* is not correlated with midlatitude positive bays, this assumption could be a reason, but they are actually correlated as will be shown later, which justifies this assumption at least for our objective).

Regarding the constitution of the SCW system, there is another ongoing issue, which concerns the coexistence of the R2 sense current wedge system with the conventional R1 sense wedge current system (Ohtani et al., 2018, 2020). However, as far as the latter dominates the former, the midlatitude northward magnetic component changes positively within the longitudinal extent of the SCW with its peak around the

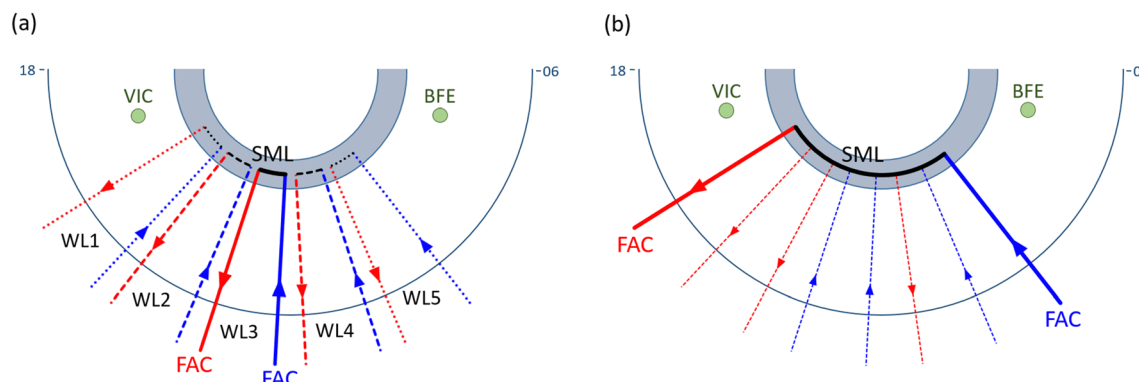


Figure 1. Illustration of two different ideas about the SCW in the polar view: (a) the SCW is an ensemble of wedgelets; and (b) the SCW is a globally coherent system. The shaded half-circle belt is the auroral zone, and the red and blue radial line segments with arrows represent upward and downward FACs, respectively. In Figure 1a the SCW consists of five wedgelets (WL1–5). WL3 is the most intense, and therefore, the *SML*-contributing wedgelet. In Figure 1b, although the SCW has internal structures as schematically depicted by thin dotted FAC lines, their contributions to the overall current system is not essential, and *SML* serves as a measure of the total current of the SCW. The small green circles represent two ground stations, Victoria (VIC) and Brorfelde (BFE), which were located at dusk and dawn, respectively, in the 15 September 1998 event (section 2).

meridional center of the WEJ enhancement, whereas the eastward component changes positively and negatively on its duskside and dawnside, respectively, as expected from the conventional SCW model (Clauer & McPherron, 1974). Therefore, we set this issue aside in the present study and use the term “substorm current wedge (SCW)” interchangeably with the substorm current system.

In the following we examine the correlation of midlatitude positive bays with *SML* and seek to address the longitudinal structure of the corresponding current system. In section 2 we examine a substorm event that took place on 15 September 1998 with a focus on magnetic variations observed at two ground stations in the subauroral zone. In section 3 we statistically examine substorm-related magnetic variations observed at these two stations. We discuss the results in section 4 and summarize the overall study in section 5.

2. The 15 September 1998 Event

In this section we examine an event that took place on 15 September 1998; we chose this old event for our event study because global auroral images are available, which, along with ground magnetometer data, allow addressing the polar distribution of substorm activity. Figure 2c shows the *SMU* (blue) and *SML* (red) indices during the 3 hr interval of 0200–0500 UT on 15 September 1998. *SMU* and *SML* are equivalent to the *AU* and *AL* indices, respectively, but based on data from all available ground stations at 40° to 80° in magnetic latitude (*MLat*), typically 120–140 stations for recent years but fewer going back in time, and provided to the SuperMAG database (Gjerloev, 2012; Newell & Gjerloev, 2011). Figure 2d shows time-shifted interplanetary magnetic field (IMF) data obtained by the Geotail (solid) and Wind (dotted) satellites around $(27, -13, 4)$ and $(181, 8, -9) R_E$, respectively, in geocentric solar magnetospheric (GSM) coordinates. The excellent agreement between the two spacecraft, despite their large separation, suggests that the observed IMF structures extended in *Y-Z* and interacted with the magnetosphere.

IMF B_Z changed sharply from northward to southward at 0226 UT, and subsequently *SML* decreased suggesting the initiation of a substorm; IMF B_Z was mostly negative during 0100–0200 UT (not shown), and the magnetosphere might already be metastable when it was hit by this southward turning. After a transient recovery, *SML* started to decrease again at 0314 UT, followed by another intensification at 0341 UT; we actually identified those start times by cross-examining global auroral images as will be described next. *SML* reached ~ -500 nT around 0400 UT. IMF B_Z started to change sharply from southward to northward at 0410 UT, and *SML* started to recover. Throughout this 3 hr period, the *SML* values were registered at ground stations in the nightside auroral zone (Figures 2a and 2b), although the location of the corresponding station jumped around especially after the 0341 UT intensification.

Figure 3 shows Polar/VIS auroral images taken before and after the start of each electrojet intensification. The green vectors represent equivalent currents deduced from ground magnetic disturbances. At each

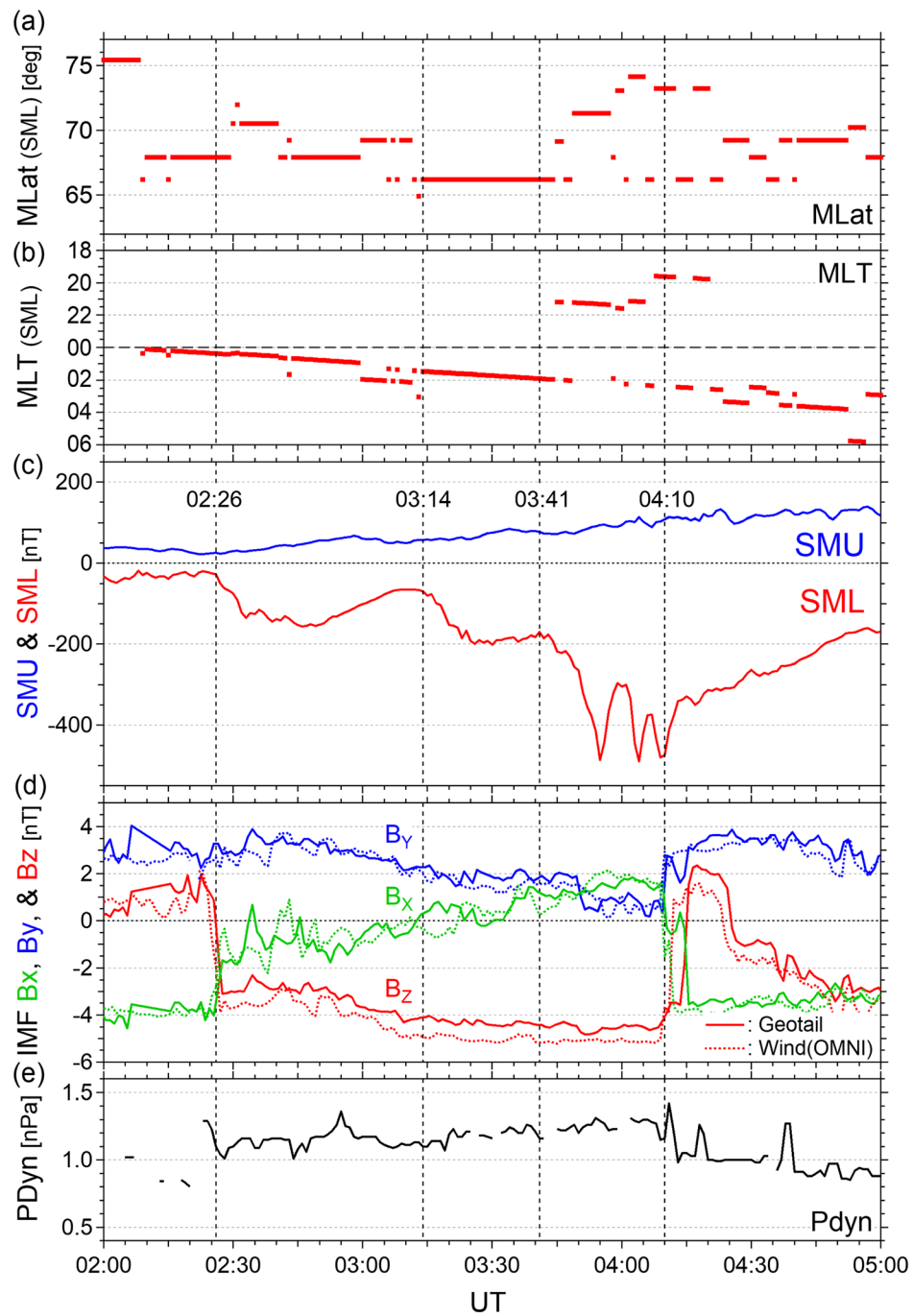


Figure 2. The (a) *MLat* and (b) *MLT* of ground stations that contributed to *SML*, (c) *SMU* (blue) and *SML* (red) indices, (d) IMF *B_X* (green), *B_Y* (blue), and *B_Z* (red) components in *GSM* observed by the *Geotail* (solid) and *Wind* (dotted) satellites, and (e) solar-wind dynamic pressure measurements by *Wind* during the interval 0200–0500 UT on 15 September 1998. The *Geotail* measurements are shifted by 5 min taking into account the propagation from its position, $(27.2, -12.7, 3.5) R_E$ in geocentric solar magnetospheric (*GSM*) coordinates, to the dayside high-latitude ionosphere. The *Wind* measurement, for which we used the *OMNI* data set, were originally propagated from the *Wind* position around $(181, 8, -9) R_E$ in *GSM* to the subsolar bow shock and are also shifted by additional 5 min. The four vertical dotted lines mark the substorm onsets/intensifications at 0226, 0314, and 0341 UT and the start of the *SML* recovery at 0410 UT.

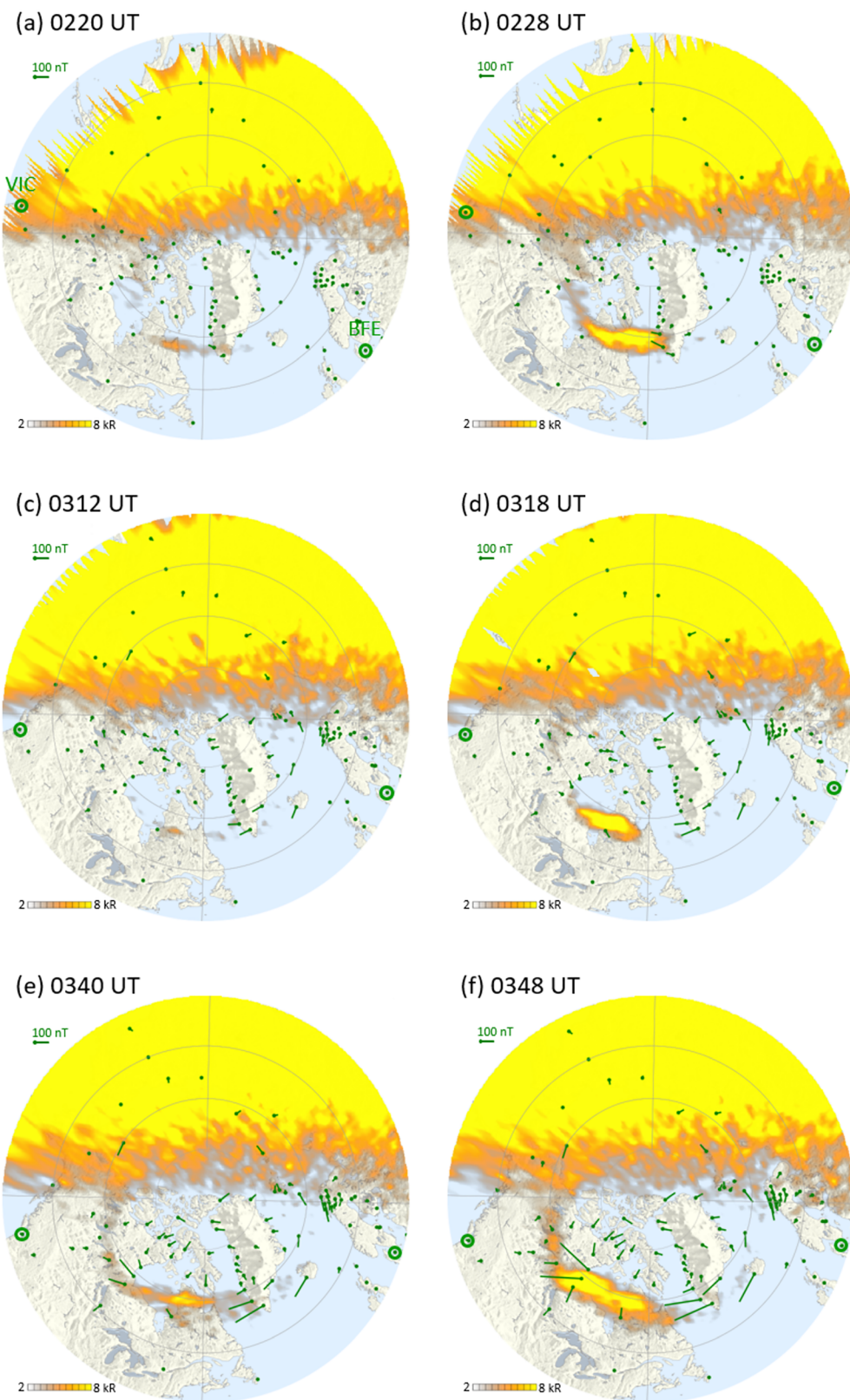


Figure 3. Polar/VIS auroral images before (left) and after (right) the (a, b) 0225, (c, d) 0314, and (e, f) 0341 UT onsets along with equivalent currents. Victoria (VIC) and Brorfelde (BFE) stations are marked by the small green circles. Sun is to the top.

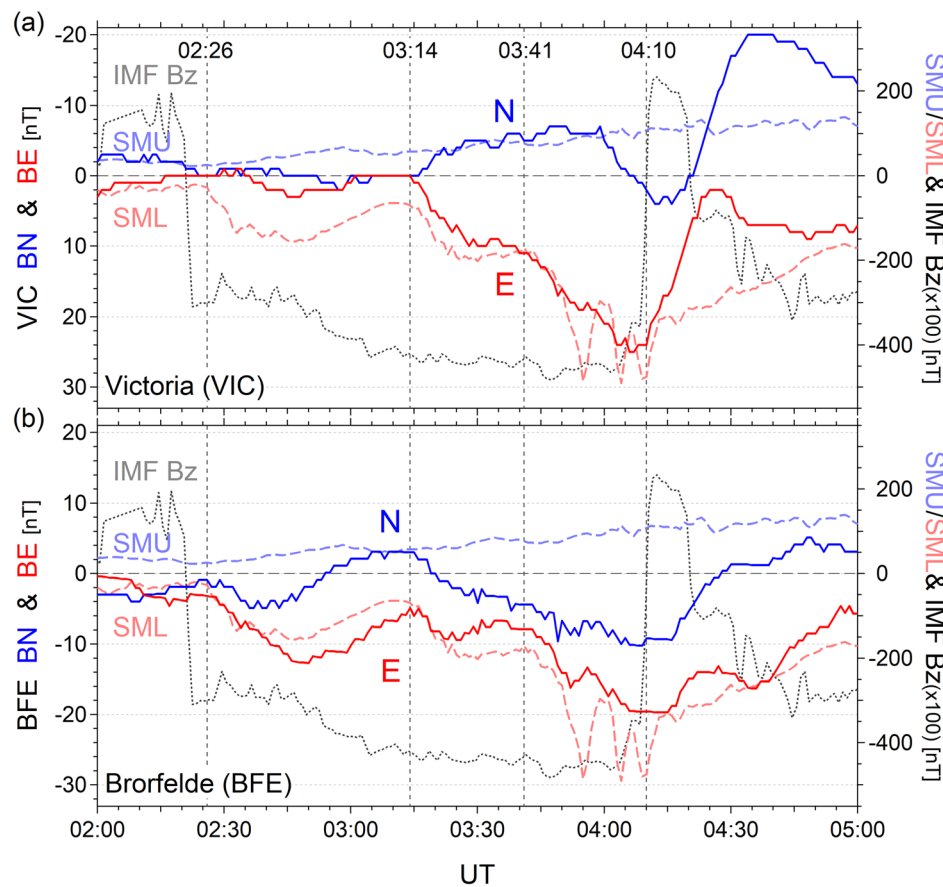


Figure 4. N (solid blue) and E (solid red) magnetic components measured at (a) VIC and (b) BFE along with SMU (dashed blue), SML (dashed red), and time-shifted IMF B_Z (dotted gray; measured by Geotail) during the interval 0200–0500 UT on 15 September 1998. The left axis of Figure 4a is inverted.

enhancement of the WEJ, the auroral emission enhanced in the premidnight sector initially in a localized area, and then, it expanded longitudinally as well as poleward. The auroral enhancement was more significant for the third intensification than the two preceding ones. Whereas the peak of the WEJ stayed at post-midnight for the first two intensifications, it jumped to premidnight (Figure 2b) and reached most poleward for this third intensification (Figure 2a).

In this event study as well as the statistical study in section 3, we use 1 min averages of magnetic field measurements made at two midlatitude ground stations, Victoria (VIC; 53.8°N in $MLat$, and 123.4°W and 48.5°N in geographic longitude ($GLon$) and latitude ($GLat$), respectively) and Brorfelde (BFE; $MLat = 52.1^\circ\text{N}$, $GLon = 11.7^\circ\text{E}$ and $GLat = 55.6^\circ\text{N}$). Figures 4a and 4b show the N (blue) and E (red) component signatures at VIC and BFE, respectively. N and E are horizontal magnetic disturbances parallel (northward) and perpendicular (eastward) to the background magnetic field, respectively (Gjerloev et al., 2012). Also plotted are SMU (dashed blue), SML (dashed red), and IMF B_Z (gray; 100 times the Geotail measurement). For VIC (Figure 3b) the left axis is inverted. Whereas VIC was located at dusk in this event, BFE was located at dawn; their locations are marked by the small green circles in Figure 3.

E is well correlated with SML at each station except that its bump at 0410–0435 UT appears to be correlated with a transient northward turning of IMF B_Z rather than with SML . This E bump may be a remote effect of the associated change of dayside FACs. Otherwise, the eastward ($E > 0$) deflection at VIC and the westward ($E < 0$) deflection at BFE roughly follows SML from the first enhancement at 0226 UT to its peak at 0410 UT. The correlation coefficient (c.c.) between E and SML from -15 to $+45$ min from the onset is -0.558 for VIC and 0.895 for BFE. If these E variations are remote effects of FACs, the FAC polarity is upward at dusk and downward at dawn as expected from the SCW model. Note that N is also correlated with SML to some extent.

These results do not necessarily mean that the SCW extended from VIC to BFE, which were separated by ~ 10 hr in MLT across midnight, but the magnetic disturbances observed at these stations can be remote effects of FACs distributed closer to midnight; this remark may apply especially to BFE since the amplitude of the N variations was comparable to that of the E variation there. However, the results indicate that in this event, the current system corresponding to the maximum WEJ intensity (as identified by SML) represented the entire nightside, and no other current system caused any comparable magnetic disturbance at VIC or BFE.

3. Statistical Study

In the 15 September 1998 event, the magnetic disturbances observed at dawn and dusk were well correlated with SML as if SML represents the entire substorm current system on the nightside. In this section we seek to address the generality of this result by statistically examining correlation between midlatitude positive bays and SML during isolated substorms.

For selecting substorm events we identified isolated substorm onsets with the SML index. The details of the identification procedure are described in Appendix A, and the list of the identified onsets is available in the supporting information. The list includes more than 14,700 substorm onsets during 1995–2018, and by requiring that the peak of the WEJ (i.e., SML -contributing ground stations) stayed on the nightside ($18 \leq \text{MLT} \leq 06$) for 45 min after the onsets, we down-selected $\sim 9,600$ events, which constitute the event base of this statistical study. We examine, as a function of MLT, the variations of N and E observed at VIC and BFE, the two ground stations we used in section 2. Data from those stations are available almost continuously throughout the interval.

Figure 5 shows the changes of N (top) and E (bottom), ΔN and ΔE , at VIC (left) and BFE (right) after substorm onsets as a function of MLT. ΔN is the change of N between the substorm onset ($t = 0$) and $t = t_{\text{peak}}$, the time at which SML reached its minimum during $0 < t \leq 45$ min, and ΔE is the same but for E . The MLT of the ground station is the median during $0 \leq t \leq t_{\text{peak}}$. The three lines represent the median and the range of the central 68.3 percentile (i.e., ± 1 standard deviation if the distribution is normal) for each 1 hr wide MLT bin.

ΔN is mostly positive in the midnight sector, whereas it tends to be slightly negative around dawn and dusk (Figures 5a and 5b). ΔE is mostly positive (eastward) and negative (westward) before and after midnight, respectively (Figures 5c and 5d). These MLT dependences of the ΔN and ΔE signatures are consistent with the SCW model (Clauer & McPherron, 1974). We also note that the magnitude of positive ΔE before midnight tends to be larger than that of negative ΔE after midnight, which suggests that the upward FAC of the SCW is more intense than the downward FAC, and accordingly, it is more confined in longitude.

It appears that ΔN peaks before midnight both at VIC and BFE (Figures 5a and 4b), and the sign of ΔE changes at premidnight at VIC (Figure 5c). These results suggest that the SCW tends to be centered at premidnight. ΔE at BFE changes its sign slightly after midnight (Figure 5d), which might reflect the distribution of ground stations. In the sector of BFE, the auroral zone is covered most densely by Scandinavian stations, which are located to the east of BFE. Accordingly, substorm onsets are identified preferentially when they take place downward of BFE, which creates a positive bias of ΔE at BFE. In contrast, the auroral zone of the VIC sector is covered by Alaskan and Canadian stations more symmetrically in longitude.

We also note that the distribution of events is not uniform in MLT. There are noticeably fewer events around $\text{MLT} = 9$ for VIC, and around $\text{MLT} = 19\text{--}20$ for BFE. Those two MLT ranges correspond to the UT window when we have very few ground stations in the premidnight sector, where substorm onsets tend to take place. In contrast, when VIC is at dusk and BFE is at dawn, the midnight sector is well covered by stations in North America and Greenland (see Figure 3), which is favorable not only for identifying substorm onsets but also for using SML as a measure of the peak WEJ intensity.

Now we examine correlation between midlatitude magnetic disturbances and SML during the 1 hr window from $t = -15$ to $+45$ min. In the rest of this study, we focus on events in which SML changed by at least 200 nT within 45 min after onsets, $\Delta SML < -200$ nT. Figures 6a and 6b show, as a function of MLT, the c.c. between N and SML for VIC and BFE, respectively; the median of MLT during the same 1 hr window is taken as the MLT of each event. The color indicates the magnitude of the slope of the linear regression

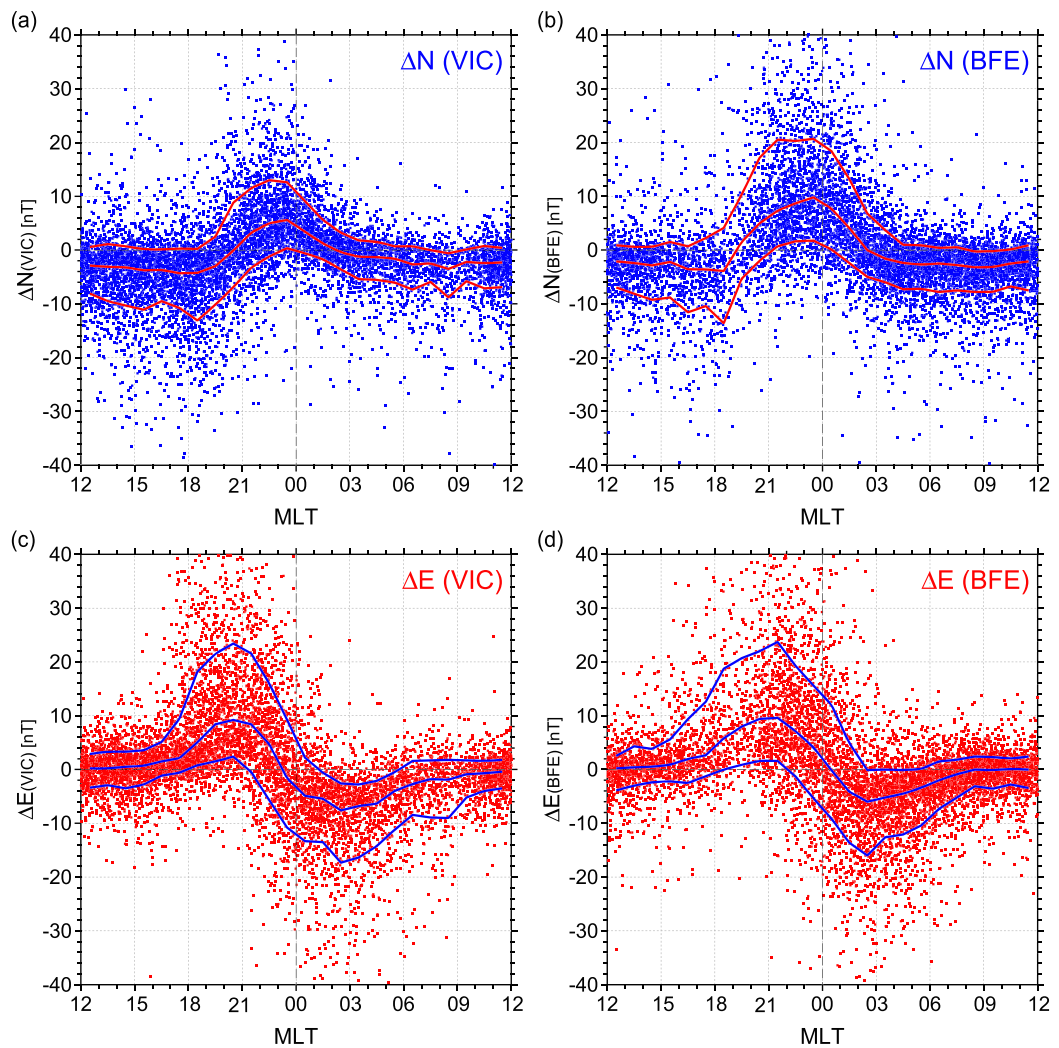


Figure 5. (a, b) ΔN and (c, d) ΔE measured at (a, c) VIC and (b, d) BFE along with the median and $\pm 1\sigma$ (as defined by the percentile) as a function of MLT. See text for details.

analysis, α_N , which represents how much N changes in nT as SML changes every nT; for example, if $|\alpha_N|$ is 0.1, $|N|$ is expected to change by 10 nT as SML changes by 100 nT. The three solid lines in each panel show the median and $\pm 1\sigma$ (as defined by the percentile). Figures 6c and 6d show the same but for E at VIC and BFE, respectively, with color indicating $|\alpha_E|$; α_E is the same as α_N but for the E variations.

N and SML are correlated negatively in the midnight sector and positively at dawn and dusk, whereas E is correlated with SML negatively before midnight and positively after midnight. Since SML decreases after substorm onsets, this result indicates that N increases near midnight but decreases away from midnight, and E changes positively (eastward) at premidnight and negatively (westward) at postmidnight, as we saw in Figure 5. Whether negative or positive, the correlation is generally high for both N and E except for the MLT ranges where the correlation changes its sign.

There are three points to note. First, the MLT center of the negative correlation between N and SML is located premidnight, suggesting that the SCW is skewed duskward. The zero crossing of the correlation between E and SML also takes place at premidnight for VIC but slightly after midnight for BFE, which may be attributed to the longitudinal distribution of auroral-zone stations as we discussed earlier. Second, $|\alpha_E|$ appears to be larger for the negative correlation at premidnight than for the positive correlation at postmidnight, which we confirmed by examining the MLT distribution of $|\alpha_E|$ (not shown). This suggests again

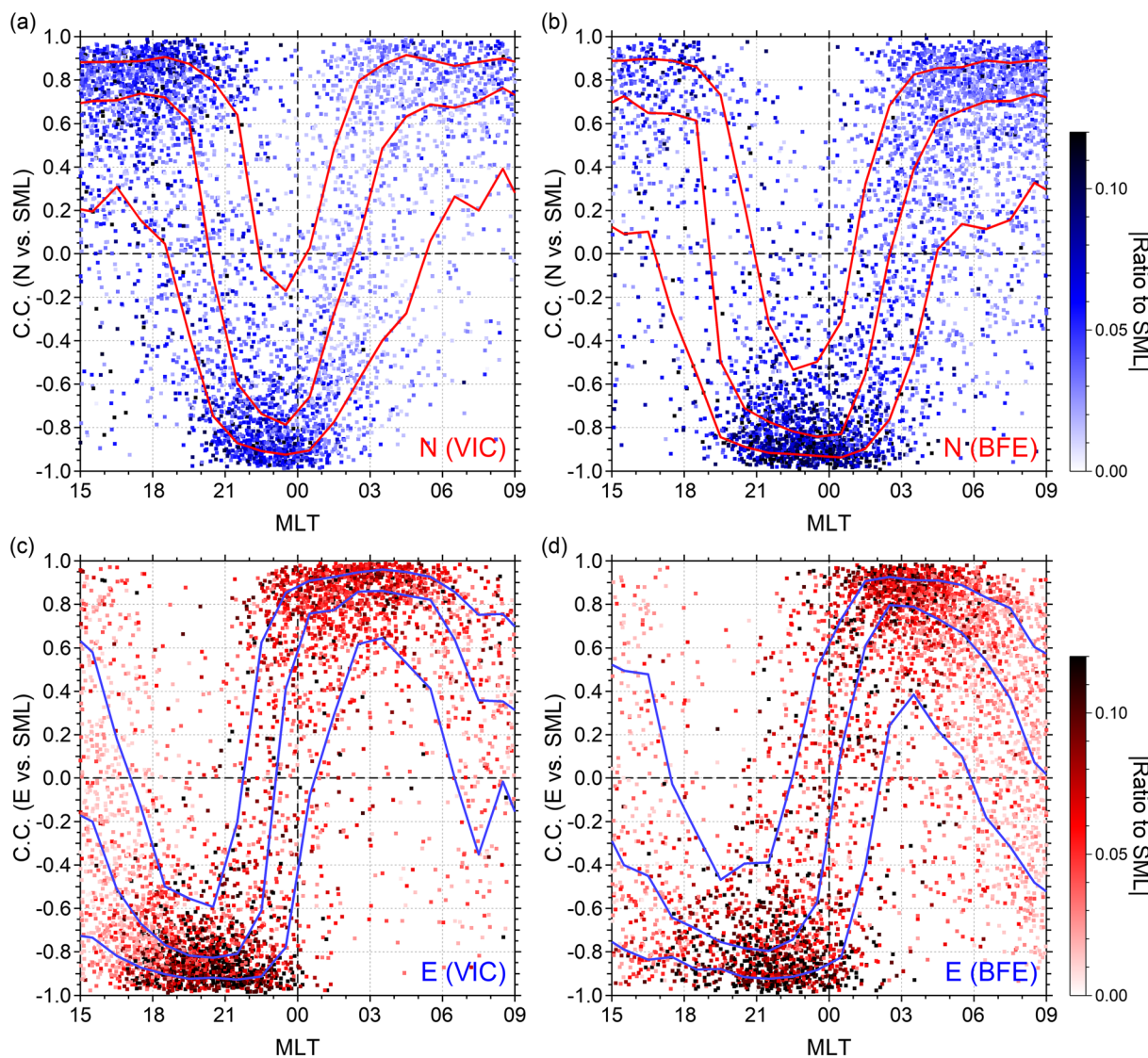


Figure 6. Correlation coefficients between *SML* and (a, b) *N* and (c, d) *E* observed at (a, c) VIC and (b, d) BFE along with the median and $\pm 1\sigma$ (as defined by the percentile) as a function of MLT. The gradation indicates the absolute value of the slope of the linear regression.

that the upward FAC on the duskside of the SCW is more confined in longitude, and therefore more intense, than the downward FAC on its dawnside. Finally, the sector of high correlation between *E* and *SML* extends several hours in MLT in both directions from midnight covering the entire nightside. This last point does not mean that the SCW extends in the same wide MLT range since the variations of *E* are generally remote effects. Instead, it strongly suggests that the current system represented by *SML*, the peak WEJ intensity, is responsible for midlatitude magnetic disturbances in the entire nightside.

We address this idea in a more direct way in terms of ΔMLT , the MLT separation from the WEJ peak, which we define for each event as the median MLT of *SML*-contributing auroral-zone stations within 45 min after the onset. Figure 7a shows the c.c. between *N* and *SML* for the VIC and BFE events combined as a function of ΔMLT . The gradation indicates $|\alpha_N|$. The solid lines show the median and $\pm 1\sigma$ (as defined by the percentile). Figure 7b is the same as Figure 7a but for *E* with the gradation for $|\alpha_E|$. The points are not distributed uniformly in ΔMLT , but they cluster reflecting the longitudinal distribution of auroral-zone stations. Since we refer to the location of the actual (equivalent) current for each event, Figure 7 should better represent the actual distribution of midlatitude magnetic disturbances than Figure 6 does.

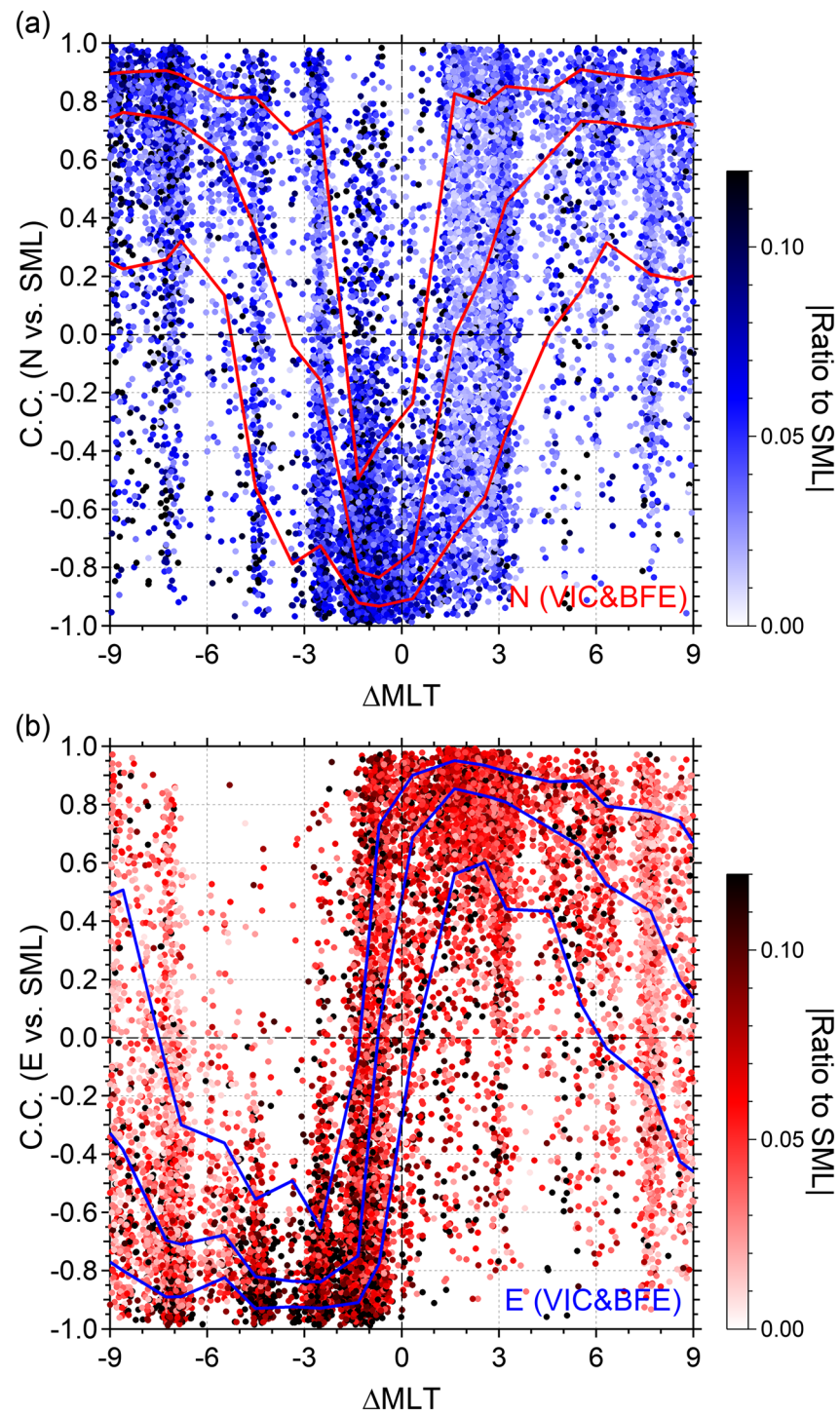


Figure 7. Correlation coefficients between *SML* and (a) *N* and (b) *E* observed at VIC and BFE along with the median and $\pm 1\sigma$ (as defined by the percentile) as a function ΔMLT , the MLT separation from the median MLT of the *SML* contributing stations within 45 min after each substorm onset. The gradation indicates the absolute value of the slope of the linear regression.

The overall pattern is consistent with the SCW model as we saw in Figure 6. However, in Figure 7, the negative c.c. between *N* and *SML* is more confined, and the c.c. between *E* and *SML* changes its sign more sharply. The longitudinal center of the wedge current is apparently located at $\Delta MLT < 0$, which may suggest that the

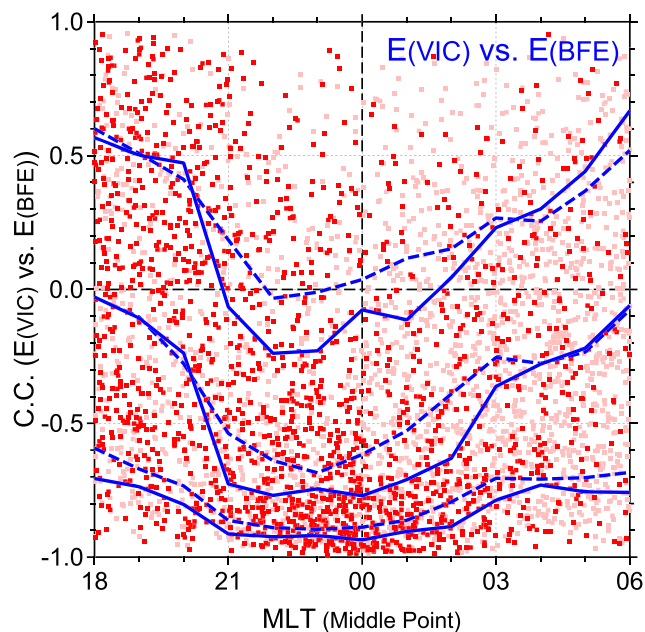


Figure 8. Correlation coefficients between E variations observed at VIC and those observed at BFE as a function of the MLT of the middle points of those two stations. The dashed lines represent the median and $\pm 1\sigma$ (as defined by the percentile) for the entire events with $\Delta SML < -200$ nT (red and faint red dots), and the solid lines are the same but for events in which $\Delta SML < -200$ nT and E varied more than 10 nT (red dots).

negatively (westward) at BFE (see Figure 5). Therefore, the correlation is expected to be negative as we found. Most importantly, the |c.c.| very often exceeds 0.7 especially for the events with large (>10 nT) E variations; the median c.c.'s are below -0.7 throughout the 5 hr wide MLT range from -3.5 to 1.5 . This result suggests that despite the 10 hr MLT separation, the E variations observed at these two stations can be attributed to the same current system. The correlation almost disappears if the midpoint is more than 3 hr away from midnight and one station is deep on the dayside. In summary, the results of our analysis consistently support the idea that as a first approximation, the SCW is one coherent system.

4. Discussion

In the previous sections we found that SML and midlatitude magnetic disturbances, either N or E , are highly correlated throughout the nightside except for the sectors of transition (Figures 6 and 7). Furthermore, when VIC is at dusk and BFE is at dawn, E variations at these two stations are also well correlated with each other despite their 10 hr separation in MLT. In general, the location of the maximum WEJ moves during the substorm expansion phase. Furthermore, FACs in any MLT sector contribute to N and E variations at midlatitudes; for example, the E variations observed at VIC and BFE after 0410 UT of the 15 September 1998 event were apparently remote effects of dayside FACs associated with the change of IMF B_Z (Figure 4). Considering these adverse factors, one may think that the correlations among the ground magnetic disturbances are even more remarkable. Our results are consistent with the idea that the substorm current system is basically a globally coherent system.

Our results may be explained alternatively if the SCW consists of wedgelets that are simultaneously formed side by side to each other and their intensities are similar; then the overall pattern of their ground magnetic effects would be the same as expected from a single global wedge. However, this idea has a couple of serious difficulties. First, the plasma flow channel, which is widely considered to be the magnetospheric counterpart of wedgelets, is a mesoscale process. The aforementioned assumption requires that they form and evolve coherently in time and space, which is not very plausible. Second, it seems that the M-I system can accommodate only a few flow channels at a given time (Ohtani, 2019). It is therefore uncertain if the substorm

upward FAC is more confined in longitude and is located farther (to the west) from the WEJ peak, whereas the downward FAC extends eastward from the WEJ peak; in this case the sign of N changes to the west of the demarcation between the upward and downward FACs. The negative and positive peaks of the c.c. between E and SML are separated by ~ 5 hr in MLT, which is consistent with the previously reported result (e.g., Clauer & McPherron, 1974) and may be considered as the longitudinal extent of the substorm current system. Most importantly, the c.c. is high throughout the entire nightside except transition ranges where the sign of the c.c. changes. It is therefore suggested that SML represents the entire nightside current system rather than one of its constituents (i.e., wedgelets).

Finally, we directly compare magnetic variations observed at VIC and BFE. Figure 8 shows the c.c. of E variations at these two stations as a function of the MLT of the middle point. The c.c.'s for the entire set of events with $|\Delta SML| > 200$ nT are shown by either faint or solid red points along with the dashed blue lines representing their median and $\pm 1\sigma$ (as defined by the percentile). We made a subset of events additionally requiring that E varied more than 10 nT at both stations. The c.c.'s for this subset are shown by the solid red points along with the solid blue lines representing their median and $\pm 1\sigma$. For this subset we expect that substorm-related E variations were more manifest.

The correlation is predominantly negative when the middle point is within a few hours from midnight. If the middle point is near midnight, VIC and BFE are located at dawn and dusk, respectively, and it is expected that E changes positively (eastward) at VIC and nega-

current system, which is several hours wide in MLT (Figure 7), can be always filled with wedgelets, which is typically 1 hr wide in MLT (Juusola et al., 2009).

Liu et al. (2015) examined FACs associated with dipolarization fronts, the magnetic feature of plasma sheet flow channels, and they found that earthward and tailward FACs are not balanced for each dipolarization front, but there is a finite net FAC, which tends to flow earthward and tailward in the postmidnight and pre-midnight sectors, respectively. It is therefore expected that there is a net ionospheric closure current flowing from postmidnight to premidnight, which contributes to the WEJ. However, the results of the present study suggest that the substorm-related WEJ can be attributed largely to a more globally coherent process.

The most critical question is how our results can be reconciled with the perception that the bursty transport of plasma and magnetic flux plays a critical role in substorm dynamics. We note that the role of bursty flows in substorm dynamics has been addressed mostly in the context of the substorm initiation (see, e.g., a review article by Kepko et al., 2015). However, most of fast flows actually do not reach geosynchronous orbit (Ohtani et al., 2006), which is well explained in terms of the flux tube entropy, pV^{γ} , of the earthward moving flux tube relative to the radial profile of background pV^{γ} (Dubyagin et al., 2011; Kim et al., 2012). Even if the SCW is initially formed by the penetration of a fast flow deep into the near-Earth region, the local pV^{γ} decreases in association with dipolarization, which makes it more difficult for subsequent plasma flows to reach the near-Earth region. The process may be envisioned as the tailward pile up of magnetic flux (Gabrielse et al., 2019).

If the dipolarization region continuously expands tailward at a few hundred km/s (e.g., Ohtani et al., 1992), within several minutes its tailward front reaches $X = -20 R_E$ or any X distance beyond which the closed magnetic flux accounts only for a very small fraction of the total closed magnetic flux in the plasma sheet. An empirical magnetic field model also shows that within 10 min after substorm onsets, the equatorial magnetic field recovers to the levels at the start of the growth phase or even overshoots (Stephens et al., 2019). In the ionosphere, the region of auroral intensification expands poleward following the auroral breakup, which typically starts several degrees equatorward of the open-closed boundary but reaches the boundary in several minutes (Friedrich et al., 2001). Therefore, these initial processes take only a small fraction of the substorm expansion phase, and for the rest of the expansion phase, the tail magnetic configuration, and therefore the M-I current system, should be rather different from the one at the substorm onset. Since the time window of our correlation analysis ranges from -15 to $+45$ min, and N and E change mostly after substorm onsets, the results of the present study reflect the substorm process at this later stage rather than the one at the onset of substorms.

Once the near-Earth magnetic field gets dipolarized, convection flows coming from farther down the tail probably divert toward the dawn and dusk flanks without reaching the near-Earth region. In addition, plasma flows also deflect vertically away from the neutral sheet carrying a significant fraction of kinetic and thermal energy along, rather than across, the magnetic field, which is partially deposited into the ionosphere around the poleward boundary of the auroral bulge in the form of intense auroral precipitation and Poynting flux (Ohtani, 2019). In general, the FACs in the plasma sheet boundary layer intensify during substorms, and they have the same polarity as the SCW (Ohtani et al., 1988). Thus, the globally coherent component of the SCW, except for the very initial period of the substorm expansion phase, probably originates far tailward of the region where the SCW initially forms. This does not mean in any sense that there is no FAC source closer to Earth. In fact, there must be numerous mesoscale and small-scale FACs that originate in the near-Earth region and even a large-scale FAC (e.g., R2 currents). However, the result of the present study suggests that they are not essential constituents of the SCW during the substorm expansion phase.

Finally, we would like to address one issue that is relevant to the subject of the present study, that is, a possible disconnection of premidnight and postmidnight WEJs. Gjerloev and Hoffman (2014) created an empirical model of substorm time equivalent currents, in which there appear to be two WEJs, one at premidnight and another at postmidnight. The WEJ at premidnight is more intense and is located at higher latitudes than the postmidnight one. The authors suggested that there may be two wedge current systems corresponding to each WEJ. If the nightside WEJ indeed consists of two separate wedge current systems, our results suggest that the intensities of those two wedge currents are correlated throughout the substorm expansion phase. One possibility is that the SCW itself is a single process, but two separate WEJs exist because the ionospheric conductance is different at premidnight and postmidnight. Another possibility is

that the premidnight and postmidnight wedge current systems actually represent two separate magnetospheric processes. Interestingly, during geomagnetic storms, an intense wedge current system recurrently forms around midnight and extends downward (Ohtani et al., 2018), suggesting that there is a certain process that drives a WEJ in the postmidnight sector. Obviously, the issue is complex and deserves a separate dedicated study in the future.

Although the substorm current system seems to be globally coherent as presented here, the conclusion of our study is founded on indirect measurements. For addressing issues about the structure and constitution of the substorm current system, direct measurements of the WEJ as well as detailed observations of mesoscale FACs are highly desirable, for which, however, we have to wait for future observations.

5. Summary

In this study we observationally tested the idea that the SCW is an ensemble of wedgelets. For the 15 September 1998 event we found that the midlatitude eastward and westward magnetic deflections observed at dusk and dawn, respectively, were not only consistent with the SCW model but also well correlated with the *SML* index suggesting that the associated M-I current system is coherent over the entire nightside. We statistically examined *N* and *E* variations observed at VIC and BFE during isolated substorms and confirmed that this result is general. Most importantly, we found that (1) the *N* and *E* variations are highly correlated with *SML* even far from midnight; (2) the c.c.'s between midlatitude magnetic variations and *SML* are spatially organized by the MLT of the maximum WEJ intensity (as identified by *SML*), and their longitudinal structures are consistent with the SCW model; and (3) the eastward *E* variations at dusk (as observed at VIC) and westward *E* variations at dawn (as observed at BFE) are well correlated with each other despite the 10 hr MLT separation of those ground stations. These results strongly suggest that as a first approximation, the substorm current system is a globally coherent system rather than an ensemble of wedgelets, although they do not preclude in any sense the existence of wedgelets or substructures of the SCW. This global system may evolve from a wedgelet formed at a substorm onset. However, for most of the subsequent expansion phase, wedgelets are probably not a primary constituent of the SCW. We suggested that the substorm current system becomes globally coherent as the plasma sheet region of energy release retreats tailward and energy is deposited primarily into the poleward boundary of the auroral bulge.

Appendix A

In this appendix we describe a technique we used to identify the onsets of substorms with the *SML* index. This technique is not meant to identify every substorm onset but rather to identify the onsets of isolated substorms. A similar technique was previously developed by Newell and Gjerloev (2011), who provided a complete list of substorms that could be used for statistical studies. However, we later found that their technique misidentified some events, and the onset timing was approximate. These shortcomings led us to develop a new technique with the purpose of providing a list of isolated events with a high degree of confidence.

Onsets are identified using a three-step approach shown in Figure A1. In Step 1 we smooth the *SML* index using a 9 min wide boxcar filter. This minimizes the impact of any short-duration variations.

Step 2 identifies possible onsets using six criteria. If *SML* at time *T* obeys these six criteria, a point is identified as a possible onset:

1. Isolated substorm ($-40 \text{ min} \leq T \leq -1 \text{ min}$): $SML \geq -100 \text{ nT}$
2. Growth phase slope ($-40 \text{ min} \leq T \leq -1 \text{ min}$): $|\Delta SML/\Delta t| \leq 1.5 \text{ nT/min}$
3. Onset break ($-10 \text{ min} \leq T \leq 10 \text{ min}$): $\Delta^2 SML/\Delta t^2 \leq -1.5 \text{ nT/min}^2$
4. Expansion phase slope ($1 \text{ min} \leq T \leq 10 \text{ min}$): $\Delta SML/\Delta t \leq -3.0 \text{ nT/min}$
5. Duration of substorm: duration $\geq 30 \text{ min}$, with $SML \leq 1.1 \cdot SML(T = 0)$
6. Intensity of substorm: $SML - SML(T = 0) \leq -100 \text{ nT}$

Figure A1 illustrates these six criteria, and below we explain why these criteria are used and how they are implemented. Criterion (1) ensures that the identified event is isolated. To minimize the impact of spikes, a linear least squares fit is made to *SML* for $-40 \text{ min} \leq T \leq -1 \text{ min}$, and it is required that the fitted values are larger than -100 nT . The threshold value -100 nT is consistent with the past studies of the substorm growth phase (e.g., Gjerloev et al., 2007). Criterion (2) ensures a gradual growth phase signature, while

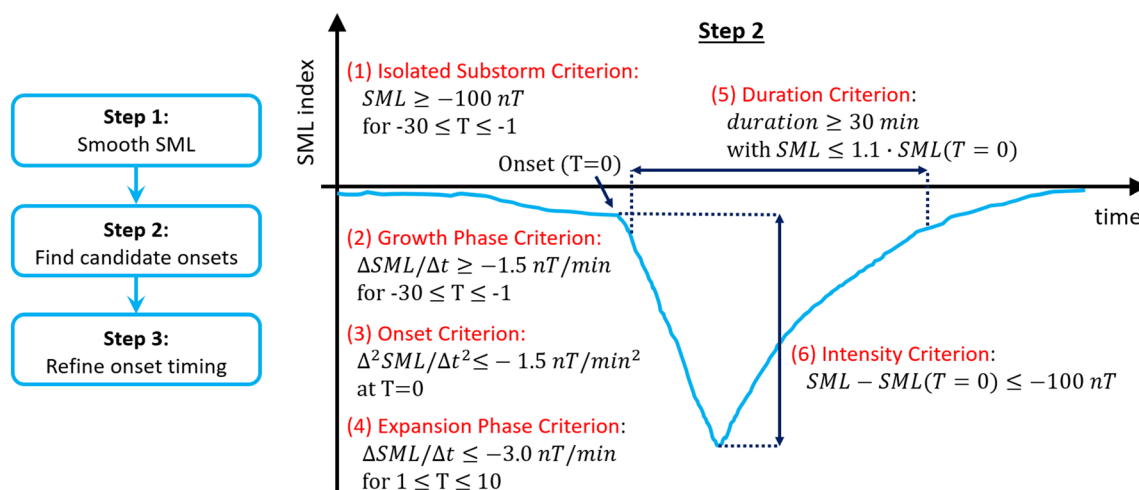


Figure A1. Schematic explanation of Step 2 of the substorm onset identification procedure.

Criterion (3) represents the well-known break in SML , which has been historically used to visually identify an onset. For robustness, $\Delta^2 SML / \Delta t^2$ is calculated based on two linear least squares fits to the 10 min windows preceding and following the onset. Criterion (4) requires the slope of SML to be steeper than -3.0 nT/min for 10 min after the onset. Again, a linear fit is used. We adopted the 10 min window since this is the low end of an expansion phase duration (Gjerloev et al., 2007). Criterion (5) requires the duration of the substorm expansion phase through the recovery phase to be $\geq 30 \text{ min}$. Finally, Criterion (6) ensures that SML decreases by at least 100 nT from the value at the onset, which is consistent with an average substorm SML reduction of 400 nT (e.g., Gjerloev et al., 2007). This approach typically provides a string of sequential points all obeying these six criteria. For example, for the event shown in Figure 2, 11 sequential candidate points satisfy these six criteria.

Step 3 refines the onset by selecting a single point among the sequential string of candidates and ensuring that the SML -contributing station is located in the midnight sector (20 MLT to 03 MLT) (Gjerloev et al., 2004; 2007). First, the onset is selected among the string of candidates as the point with the minimum second derivative (i.e., the maximum of its amplitude). Second, the SML -contributing station is required to be located in the midnight region by selecting the earliest time following this onset, $T \in [0, 15]$, for which the SML -contributing station is located in 20 MLT to 03 MLT region. It should be noted that the SML -contributing stations are often located on the dayside during the substorm growth phase (Gjerloev et al., 2004). If the difference between preliminary onset and final onset exceeds 15 min, the event is classified as a dayside event and is thus not a substorm.

The technique was validated independently by each author of this paper with a visual inspection. A typical number of substorms identified by this technique is 500–700/year. It is again important to note that this technique selects isolated clear substorms, and it is not meant to be complete in any sense. For example, in the event shown in Figure 2 the technique identifies the first onset at 2:26 UT, whereas the subsequent events are categorized as intensifications, rather than isolated substorms, and therefore are not selected by this procedure. The entire substorm list is available in the supporting information, and it is also posted at the SuperMAG website where it will be routinely updated as new data are ingested.

Data Availability Statement

Those ground magnetometer data were provided through the SuperMAG website (<http://supermag.jhuapl.edu/>) after its standard processing. The SMI and SML indices and polar diagrams of equivalent currents along with Polar/VIS images are also available at the SuperMAG website. SuperMAG is an international collaboration with many organizations and institutes, and it is funded by National Science Foundation (NSF). The OMNI data were provided by the GSFC/SPDF OMNIWeb (at <https://omniweb.gsfc.nasa.gov>). Geotail

magnetometer data were provided by S. Kokubun and T. Nagai and are available online (at <https://darts.isas.jaxa.jp/index.html.en>).

Acknowledgments

We thank Canadian Magnetic Observatory System for the Victoria magnetometer data and Danish Technical University Space for the Brorfelde magnetometer data. Support for this research at the Johns Hopkins University Applied Physics Laboratory was provided by National Aeronautics and Space Administration (NASA) grant NNX16AF74G (SO) and National Science Foundation (NSF) grants 1502700 (S. O.), 1603028 (S. O.), and 1417899 (J. W. G.).

References

- Akasofu, S.-I. (1964). The development of the auroral substorm. *Planetary and Space Science*, 12(4), 273–282. [https://doi.org/10.1016/0032-0633\(64\)90151-5](https://doi.org/10.1016/0032-0633(64)90151-5)
- Akasofu, S.-I. (1972). Magnetospheric substorms: A model. In E. R. D. Reidel (Ed.), *The Magnetosphere, Solar Terrestrial Physics; Part 3* (pp. 131–151). Dordrecht(Holland)/Boston(USA).
- Akasofu, S.-I., Chapman, S., & Meng, C.-I. (1965). The polar electrojet. *Journal of Atmospheric and Terrestrial Physics*, 27(11-12), 1275–1305. [https://doi.org/10.1016/0021-9169\(65\)90087-5](https://doi.org/10.1016/0021-9169(65)90087-5)
- Clauer, C. R., & McPherron, R. L. (1974). Mapping the local time-universal time development of magnetospheric substorms using mid-latitude magnetic observations. *Journal of Geophysical Research*, 79(19), 2811–2820. [http://doi.org/10.1029/ja079i019p02811](https://doi.org/10.1029/ja079i019p02811)
- Dubyagin, S., Sergeev, V., Apatenkov, S., Angelopoulos, V., Runov, A., Nakamura, R., et al. (2011). Can flow bursts penetrate into the inner magnetosphere? *Geophysical Research Letters*, 38, L08102. [http://doi.org/10.1029/2011gl047016](https://doi.org/10.1029/2011gl047016)
- Friedrich, E., Samson, J. C., Voronkov, I., & Rostoker, G. (2001). Dynamics of the substorm expansive phase. *Journal of Geophysical Research*, 106(A7), 13,145–13,163. <https://doi.org/10.1029/2000JA000292>
- Fujii, R., Hoffman, R. A., Anderson, P. C., Craven, J. D., Sugiura, M., Frank, L. A., & Maynard, N. C. (1994). Electrodynamic parameters in the nighttime sector during auroral substorms. *Journal of Geophysical Research*, 99(A4), 6093–6112. <https://doi.org/10.1029/93JA02210>
- Fukushima, N. (1971). Electric current systems for polar substorms and their magnetic effect below and above the ionosphere. *Radio Science*, 6(2), 269–275. <https://doi.org/10.1029/RS006i002p00269>
- Gjerloev, J. W. (2012). The SuperMAG data processing technique. *Journal of Geophysical Research*, 117, A09213. [http://doi.org/10.1029/2012ja017683](https://doi.org/10.1029/2012ja017683)
- Gjerloev, J. W., & Hoffman, R. A. (2014). The large-scale current system during auroral substorms. *Journal of Geophysical Research: Space Physics*, 119, 4591–4606. <https://doi.org/10.1002/2013JA019176>
- Gjerloev, J. W., Hoffman, R. A., Friel, M., Frank, L. A., & Sigwarth, J. B. (2004). Substorm behavior of the auroral electrojet indices. *Annales de Geophysique*, 22(6), 2135–2149. <https://doi.org/10.5194/angeo-22-2135-2004>
- Gjerloev, J. W., Hoffman, R. A., Sigwarth, J. B., & Frank, L. A. (2007). Statistical description of the bulge-type auroral substorm in the far ultraviolet. *Journal of Geophysical Research*, 112, A07213. <https://doi.org/10.1029/2006JA012189>
- Gabrielse, C., Spanswick, E., Artemyev, A., Nishimura, Y., Runov, A., Lyons, L., et al. (2019). Utilizing the Heliophysics/Geospace System Observatory to Understand Particle Injections: Their Scale Sizes and Propagation Directions. *Journal of Geophysical Research: Space Physics*, 124, 5584–5609. [http://doi.org/10.1029/2018ja025588](https://doi.org/10.1029/2018ja025588)
- Henderson, M. G. (2013). Auroral substorms, poleward boundary activations, auroral streamers, omega bands, and onset precursor activity. In A. Keiling, E. Donovan, F. Bagenal, T. Karlsson (Eds.), *Auroral Phenomenology and Magnetospheric Processes: Earth and Other Planets* (39–54). Washington, DC: American Geophysical Union. <https://doi.org/10.1029/2011GM001165>
- Juusola, L., Nakamura, R., Amm, O., & Kauristie, K. (2009). Conjugate ionospheric equivalent currents during bursty bulk flows. *Journal of Geophysical Research*, 114, A04313. <https://doi.org/10.1029/2008JA013908>
- Kepko, L., McPherron, R. L., Amm, O., Apatenkov, S., Baumjohann, W., Birn, J., et al. (2015). Substorm current wedge revisited. *Space Science Reviews*, 190(1-4), 1–46. <https://doi.org/10.1007/s11214-014-0124-9>
- Kim, H.-S., Lee, D.-Y., Ohtani, S., Park, M.-Y., & Ahn, B.-H. (2012). On near-tail bubble penetration into geosynchronous altitude. *Journal of Geophysical Research*, 117, A07205. <https://doi.org/10.1029/2012JA017749>
- Kisabeth, J. L., & Rostoker, G. (1974). The expansive phase of magnetospheric substorms: 1. Development of the auroral electrojets and auroral arc configuration during a substorm. *Journal of Geophysical Research*, 79(7), 972–984. <https://doi.org/10.1029/JA079i007p00972>
- Liu, J., Angelopoulos, V., Chu, X., Zhou, X.-Z., & Yue, C. (2015). Substorm current wedge composition by wedgelets. *Geophysical Research Letters*, 42, 1669–1676. <https://doi.org/10.1002/2015GL063289>
- McPherron, R. L., Russell, C. T., & Aubrey, M. P. (1973). Satellite studies of magnetospheric substorms on August 15, 1968: 9. Phenomenological model for substorms. *Journal of Geophysical Research*, 78(16), 3131–3149. <https://doi.org/10.1029/JA078i016p03131>
- Merkin, V. G., Panov, E. V., Sorathia, K. A., & Ukhorskiy, A. (2019). Contribution of bursty bulk flows to the global dipolarization of the magnetotail during an isolated substorm. *Journal of Geophysical Research: Space Physics*, 124, 8647–8668. <https://doi.org/10.1029/2019JA026872>
- Nakamura, R., Baumjohann, W., Schödel, R., Brittmacher, M., Sergeev, V. A., Kubyshkina, M., et al. (2001). Earthward flow bursts, auroral streamers, and small expansions. *Journal of Geophysical Research*, 106(A6), 10791–10802. <https://doi.org/10.1029/2000JA000306>
- Newell, P. T., & Gjerloev, J. W. (2011). Evaluation of SuperMAG auroral electrojet indices as indicators of substorms and auroral power. *Journal of Geophysical Research*, 116, A12211. <https://doi.org/10.1029/2011JA016779>
- Obayashi, T., & Nishida, A. (1968). Large-scale electric field in the magnetosphere. *Space Science Reviews*, 8(1), 3–31.
- Ohtani, S. (2019). Substorm energy transport from the magnetotail to the nightside ionosphere. *Journal of Geophysical Research: Space Physics*, 124, 8669–8684. <https://doi.org/10.1029/2019JA026964>
- Ohtani, S., Gjerloev, J. W., Anderson, B. J., Kataoka, R., Troshichev, O., & Watari, S. (2018). DAWNside wedge current system formed during intense geomagnetic storms. *Journal of Geophysical Research: Space Physics*, 123, 9093–9109. <https://doi.org/10.1029/2018JA025678>
- Ohtani, S., Kokubun, S., Elphic, R. C., & Russell, C. T. (1988). Field-aligned current signatures in the near-tail region, 1: ISEE observations in the plasma sheet boundary layer. *Journal of Geophysical Research*, 93(A9), 9709–9720. <https://doi.org/10.1029/JA093iA09p09709>
- Ohtani, S., Kokubun, S., & Russell, C. T. (1992). Radial expansion of the tail current disruption during substorms: A new approach to the substorm onset region. *Journal of Geophysical Research*, 97(A3), 3129–3136. <https://doi.org/10.1029/91JA02470>
- Ohtani, S., Motoba, T., Gkioulidou, M., Takahashi, K., & Singer, H. J. (2018). Spatial development of the dipolarization region in the inner magnetosphere. *Journal of Geophysical Research: Space Physics*, 123, 5452–5463. <https://doi.org/10.1029/2018JA025443>
- Ohtani, S., Motoba, T., Takahashi, K., & Califff, S. (2020). Generalized Substorm Current Wedge Model: Two Types of Dipolarizations in the Inner Magnetosphere. *Journal of Geophysical Research: Space Physics*, 125, e2020JA027890. <https://doi.org/10.1029/2020JA027890>
- Ohtani, S., Singer, H. J., & Mukai, T. (2006). Effects of the fast plasma sheet flow on the geosynchronous magnetic configuration: Geotail and GOES coordinated study. *Journal of Geophysical Research*, 111, A01204. <https://doi.org/10.1029/2005JA011383>
- Rostoker, G. (1991). Some observational constraints for substorm models, magnetospheric substorms. *Geophysical Monograph Series AGU*, 64, 61–72. <https://doi.org/10.1029/GM064p0061>

- Sergeev, V. A., Liou, K., Meng, C.-I., Newell, P. T., Brittnacher, M., Parks, G., & Reeves, G. D. (1999). Development of auroral streamers in association with localized impulsive injections to the inner magnetotail. *Geophysical Research Letters*, 26(3), 417–420. <https://doi.org/10.1029/1998GL900311>
- Stephens, G. K., Sitnov, M. I., Korth, H., Tsyganenko, N. A., Ohtani, S., Gkioulidou, M., & Ukhorskiy, A. Y. (2019). Global empirical picture of magnetospheric substorms inferred from multimission magnetometer data. *Journal of Geophysical Research: Space Physics*, 124, 1085–1110. <https://doi.org/10.1029/2018JA025843>